Transition radiation from ultrarelativistic particles*

Loyal Durand
Department of Physics, University of Wisconsin, Madison, Wisconsin 53706

(Received 8 July 1974)

In the present paper, we give a simple derivation of the spectrum and angular distribution of the transition radiation emitted by ultrarelativistic particles which pass through dielectric foils. The approximations appropriate for high-frequency radiation in the ultrarelativistic limit are made at the beginning. The calculations are consequently much simpler than standard calculations, and our results, some of which are apparently new, are relatively simple and easy to interpret. The primary emphasis in the development is on conditions likely to be encountered in the application of transition radiation detectors in high-energy physics.

I. INTRODUCTION

Transition radiation is omitted whenever a charged particle crosses an interface between two media with different dielectric functions.[1] The radiation is associated with the abrupt change in the electromagnetic field of the particle in the transition, and in the case of highly relativistic particles, is emitted primarily at x-ray frequencies. In particular, a particle with $\gamma = E/mc^2 \gg 1$ which passes through a slab of material with a dielectric function

$$\epsilon(\omega) = 1 - \frac{\omega_p^2}{\omega^2}, \quad \frac{\omega_p}{\omega} \ll 1 \tag{1}$$

and a thickness $a \gg \gamma c/\omega_p$ will lose a total amount of energy

$$\mathcal{E} \sim \frac{2}{3}\frac{e^2}{c}\gamma\omega_p \tag{2}$$

in transition radiation.[2] Here ω is the angular frequency of the radiation, and ω_p is the bulk plasma frequency of the material in question, given in terms of the total number density of electrons in the material n, and the charge and mass of the electron by

$$\omega_p = \left(\frac{4\pi n e^2}{m_e}\right)^{1/2}. \tag{3}$$

For typical materials, the plasma energy $\hbar\omega_p$ is about 30 eV.

It has been recognized for some time that the linear dependence of $\mathcal{E}$ on γ would make efficient x-ray transition radiation detectors quite useful in high-energy physics for the measurement of the energies of ultrarelativistic particles, for example, TeV cosmic-ray protons, or for discrimination among particles of known momentum and different masses. The practicality of such detectors has been demonstrated in recent experiments of Wang *et al.*[3] and Alikhanian *et al.*[4] It has also been suggested recently that the transition radiation associated with the passage of cosmic-ray electrons through interstellar dust grains could be important as a source of the observed diffuse galactic x-ray radiation.[5] Although detailed calculations[6] show that this suggestion is not correct, transition radiation from dust clouds may nevertheless be of interest in special situations.

The theory of transition radiation has been studied by many authors since the existence of this radiation was pointed out in 1946 by Ginzburg and Frank.[1] Thorough reviews of the subject have been given by Bass and Yakovenko[7] and Garibian.[8] Although the physical principles involved are very simple, the calculations necessary to derive exact results in the problems which have been studied can be rather complicated, as are the results themselves. In the present paper, we will give a new derivation of the spectrum and angular distribution of the radiation emitted by ultrarelativistic particles which pass through dielectric slabs. The approximations appropriate to the ultrarelativistic limit are made at the beginning. The calculations are consequently much simpler than the standard calculations, and our results, some of which do not appear in the literature, are relatively simple and easy to interpret. The case of normal incidence of a particle on a single slab is treated in Sec. II. The modifications of these results which appear in the case of oblique incidence on a single slab, and with the multiple-slab arrangements (foil stacks) used in practical transition radiation detectors, are considered in Sec. III. Our methods can also be used quite easily to treat the emission of transition radiation at rough surfaces or from irregularly shaped objects, for example, interstellar dust grains[6] or cavities in a porous dielectric. The standard boundary-value methods are not readily adaptable to these problems.

II. NORMAL INCIDENCE ON A SINGLE SLAB

A. Derivation of the basic equations

Consider a single ultrarelativistic particle with charge e and velocity $\vec{v}$ which passes through a plane dielectric slab of thickness a. The passage of the particle results in a transient polarization of the slab, hence, in the flow of a transient polarization current and the emission of radiation. We will assume that the slab is perpendicular to $\vec{v}$, and will take the z axis of our cylindrical coordinate system along $\vec{v}$, with the origin at the point at which the particle emerges from the slab. The electric field of the particle at a point $\vec{r} = (\vec{b}, z)$ and time t (measured relative to the time of impact) is given in vacuum by the Fourier integral

$$\vec{E}(\vec{b}, z, t) = (2\pi)^{-1/2} \int_{-\infty}^{\infty} d\omega\, e^{-i\omega t}\, \vec{E}(\vec{b}, z, \omega), \tag{4}$$

where the components of $\vec{E}(\vec{b}, z, \omega)$ perpendicular and parallel to $\vec{v}$ are given by[9]

$$\vec{E}_{\perp}(\vec{b}, z, \omega) = \hat{b}\, \frac{e}{v} \left(\frac{2}{\pi}\right)^{1/2} \frac{\omega}{\gamma v} K_1\!\left(\frac{\omega b}{\gamma v}\right) e^{i(\omega/v)z} \tag{5a}$$

$$= -\frac{i}{2\pi}\, \frac{e}{v} \left(\frac{2}{\pi}\right)^{1/2} \int d^2q\, \frac{\vec{q}}{q^2 + (\omega/\gamma v)^2} \times e^{i\vec{q}\cdot\vec{b} + i(\omega/v)z}, \tag{5b}$$

$$\vec{E}_{\parallel}(\vec{b}, z, \omega) = -i\,\hat{v}\, \frac{e}{\gamma v} \left(\frac{2}{\pi}\right)^{1/2} \frac{\omega}{\gamma v} K_0\!\left(\frac{\omega b}{\gamma v}\right) e^{i(\omega/v)z} \tag{6a}$$

$$= -\hat{v}\, \frac{i}{2\pi}\, \frac{e}{\gamma v} \left(\frac{2}{\pi}\right)^{1/2} \int d^2q\, \frac{\omega/\gamma v}{q^2 + (\omega/\gamma v)^2} \times e^{i\vec{q}\cdot\vec{b} + i(\omega/v)z}. \tag{6b}$$

Here $\vec{q}$ and $\vec{b}$ are transverse with respect to $\vec{v}$, $\vec{q}\cdot\vec{v} = \vec{b}\cdot\vec{v} = 0$. For ultrarelativistic particles, the field is nearly transverse except in a very limited region close to the particle, $|\vec{E}_{\parallel}|/|\vec{E}_{\perp}| \sim 1/\gamma \ll 1$, and is strong at the angular frequency ω out to distances $b \sim \gamma v/\omega \sim \gamma c/\omega = \gamma\lambda$ from the line of flight. We will anticipate the result that the contribution of the longitudinal field $\vec{E}_{\parallel}$ to the transition radiation is of order $1/\gamma^2$ relative to the contribution of the transverse field, and will approximate $\vec{E}$ by $\vec{E}_{\perp}$ in the following calculations.

At frequencies $\omega \gg \omega_p$, the dielectric function of the slab is close to unity, $|\epsilon(\omega) - 1| \sim (\omega_p/\omega)^2 \ll 1$. We may therefore neglect both dielectric shielding in the slab and the small radiation field which is present, and approximate the electric field inside the slab by the vacuum field

$$\vec{E}_{\text{slab}}(\vec{r}, \omega) \approx \vec{E}_{\text{vac}}(\vec{r}, \omega) \approx \vec{E}_{\perp}(\vec{r}, \omega), \qquad \omega \gg \omega_p,\ \gamma \gg 1. \tag{7}$$

With this approximation, the polarization density in the slab is given by

$$\vec{P}(\vec{r}, \omega) \approx \frac{\epsilon - 1}{4\pi}\, \vec{E}_{\perp}(\vec{r}, \omega), \tag{8}$$

and the polarization current density by

$$\vec{J}(\vec{r}, \omega) = -i\omega\, \vec{P}(\vec{r}, \omega). \tag{9}$$

The vector potential set up at a point $\vec{r}'$ by this source is given formally in terms of the exact Green's function for the problem,

$$\vec{A}(\vec{r}', \omega) = \int G(\vec{r}', \vec{r}, \omega)\, \vec{J}(\vec{r}, \omega)\, d^3r, \tag{10}$$

where the integration is over the volume of the slab. At the frequencies of interest, $\omega a/c \gg 1$ for any reasonable slab thickness. We can therefore approximate the asymptotic Green's function using a combination of ray optics with a Huygens construction. We assume, in particular, rectilinear propagation of the radiation from the source point to the surface of the slab with a real wave vector $\vec{k}$, Snell's law refraction at the surface, and rectilinear propagation to the point of observation with a wave vector $\vec{k}$. Here

$$\vec{k} = \frac{\omega}{c}\,\hat{k}, \quad k_z = \frac{\omega}{c}\cos\theta, \quad \vec{k}_{\perp} = \frac{\omega}{c}\sin\theta\,\hat{k}_{\perp}, \tag{11a}$$

$$\vec{\kappa} = \epsilon^{1/2}\, \frac{\omega}{c}\,\hat{\kappa}, \quad \kappa_z = \frac{\omega}{c}\left[\epsilon - \sin^2\theta\right]^{1/2}, \quad \vec{\kappa}_{\perp} = \frac{\omega}{c}\sin\theta\,\hat{k}_{\perp}, \tag{11b}$$

where θ is the angle between the asymptotic wave vector $\vec{k}$ and the velocity of the particle $\vec{v}$.[10] We will neglect multiple reflections of the wave in the slab and changes in its amplitude at the surface, effects which are negligible for $|\epsilon - 1| \ll 1$. Furthermore, $\epsilon(\omega) < 1$ for $\omega > \omega_p$, and it is not necessary to consider the emission of Čerenkov radiation by the particle in the slab.[11] The asymptotic form of the vector potential is given in this approximation by

$$\vec{A}(\vec{r}', \omega) \underset{r' \to \infty}{\sim} \frac{1}{c}\, \frac{e^{ikr'}}{r'} \int e^{-i\vec{\kappa}\cdot\vec{r}}\, \vec{J}(\vec{r}, \omega)\, d^3r, \tag{12}$$

where the integration is again over the volume of the slab. Using (8), (9), and (5b), we find that

$$\vec{A}(\vec{r}', \omega) \underset{r' \to \infty}{\sim} -i\, \frac{\omega}{c}\, \frac{\epsilon - 1}{4\pi}\, \frac{e^{ikr'}}{r'} \times \int_{-a}^{0} dz \int d^2b\, e^{-i\vec{\kappa}\cdot\vec{r}}\, \vec{E}_{\perp}(\vec{b}, z, \omega) \tag{13a}$$

$$= \frac{i}{(2\pi)^{1/2}}\, \frac{e}{v}\, \frac{\omega}{c}\, \frac{\epsilon - 1}{(\omega/v) - \kappa_z}\, \frac{\vec{k}_{\perp}}{\kappa_{\perp}^2 + (\omega/\gamma v)^2} \times \left[1 - e^{i(\kappa_z - \omega/v)a}\right] \frac{e^{ikr'}}{r'}. \tag{13b}$$

The calculation of the asymptotic magnetic and electric fields and the Poynting flux is straightforward, and leads to the following result for the energy radiated per unit solid angle per unit angular frequency in a single traversal of the slab:

$$\frac{d^2\mathcal{E}}{d\omega d\Omega} = \frac{c}{2\pi}\,|\,i\vec{k}\times\vec{A}|^2 r'^2 \tag{14a}$$

$$= \frac{c}{2\pi^2}\left[\frac{e}{v}\,\frac{\omega}{c}\,\frac{\epsilon-1}{(\omega/v)-\kappa_z}\right]^2 \frac{|\vec{k}\times\vec{\kappa}_\perp|^2}{[\kappa_\perp^2+(\omega/\gamma v)^2]^2} \times\left[1-\cos\left(\frac{\omega}{v}-\kappa_z\right)a\right]. \tag{14b}$$

We can simplify this experssion considerably for $\gamma\gg 1$, $\omega/\omega_p\gg 1$, and θ small. In this limit,

$$\frac{\omega}{v}-\kappa_z \sim \frac{\omega}{2c}\left(\theta^2+\frac{1}{\gamma^2}+\frac{\omega_p^2}{\omega^2}\right),$$

$$\kappa_\perp^2+(\omega/\gamma v)^2 \sim \frac{\omega^2}{c^2}\left(\theta^2+\frac{1}{\gamma^2}\right), \tag{15}$$

and

$$\frac{d^2\mathcal{E}}{d\omega d\Omega} \sim \frac{2e^2}{\pi^2 c}\left(\frac{\omega_p}{\omega}\right)^4 \frac{\theta^2}{[\theta^2+(1/\gamma^2)+(\omega_p^2/\omega^2)]^2[\theta^2+(1/\gamma^2)]^2} \times\left[1-\cos\left(\frac{\omega}{v}-\kappa_z\right)a\right],$$

$$\gamma\gg 1,\ \omega/\omega_p\gg 1,\ \theta\ll 1 \tag{16}$$

where we have dropped terms of order θ^2 relative to those retained. It is clear from this expression that most of the radiation will be emitted at small angles if γ and ω/ω_p are large, hence, that the use of the small-angle approximation is justified. It is also easily checked that the error in Eq. (16) which results from our neglect of $\vec{E}_\parallel$ in Eqs. (8) and (12) is of order $1/\gamma^2$. While the radiation emitted at any fixed angle is plane-polarized, with the electric vector in the plane which contains $\vec{v}$ and $\vec{k}$, the average angle of emission is extremely small under the conditions of interest, and polarization is washed out in practical detectors which accept all or most of the radiation. We will not consider the polarization further (see, however, Ref. 8).

Equation (16) is our basic result for the distribution of high-frequency transition radiation from a single dielectric slab. This expression may be obtained from the much more complicated exact results given by Pafomov[12] and by Garibian and Chalikian[13] by taking the limits appropriate for $\gamma\gg 1$, $\omega/\omega_p\gg 1$, and $\theta\ll 1$ and dropping the terms which describe multiple internal reflections. Under the conditions of primary interest for transition radiation detectors, the cosine in the last factor in Eq. (16) oscillates rapidly with small changes in either θ or ω, and can be neglected if one considers the average intensity of the radiation in a small interval in either of these quantities. We will therefore drop this term in the following discussion. As we will show in Sec. IIE, this approximation is legitimate if the slab is thick enough that $(\omega_p a/\gamma c)\gg 1$. For a typical dielectric with a plasma energy $\hbar\omega_p \sim 30$ eV, this requires that $a\gg\gamma(0.66\times 10^{-6}$ cm). Thus,

$$\frac{d^2\mathcal{E}}{d\omega d\Omega} \sim \frac{2e^2}{\pi^2 c}\left(\frac{\omega_p}{\omega}\right)^4 \times \frac{\theta^2}{[\theta^2+(1/\gamma^2)+(\omega_p^2/\omega^2)]^2[\theta^2+(1/\gamma^2)]^2},$$

$$a\gg\gamma c/\omega_p. \tag{17}$$

This result is just twice the high-energy, high-frequency limit of the exact result for a single vacuum-dielectric interface.[14] The extra factor of 2 is associated with the second vacuum-dielectric interface in the case of slab geometry.

B. Angular distribution of radiation from a thick slab

It is clear from Eq. (17) that the transition radiation from an ultrarelativistic particle normally incident on a thick dielectric slab is azimuthally symmetric about the line of flight of the particle, and is confined to a narrow forward cone. The distribution of the radiation as a function of θ is given by

$$\frac{d^2\mathcal{E}}{d\omega d\theta} = 2\pi\theta\,\frac{d^2\mathcal{E}}{d\omega d\Omega},\quad \theta\ll 1. \tag{18}$$

This function vanishes as θ^3 for $\theta\to 0$, and has a sharp maximum for $\theta\sim 1/\gamma$. At frequencies high enough that $\omega_p/\omega\ll\gamma^{-1}$, the angular distribution of the radiation (but not its intensity) is essentially independent of ω [see Eq. (17)], $d^2\mathcal{E}/d\omega d\theta$ falls as θ^{-5} for angles large relative to γ^{-1}, and the radiation is confined to angles $\theta\lesssim\gamma^{-1}$. However, the spectral intensity of the radiation $d\mathcal{E}/d\omega$ is quite small in this limit because of the overall factor $(\omega_p/\omega)^4$ in Eq. (17). A more interesting case for practical purposes is that in which $1\gg(\omega_p/\omega)\gg\gamma^{-1}$. In this case, $d^2\mathcal{E}/d\omega d\theta$ decreases as θ^{-1} for $\gamma^{-1}\lesssim\theta\lesssim\omega_p/\omega$ and is cut off as θ^{-5} only for $\theta\gg\omega_p/\omega$. The angular distribution of the radiation is consequently much broader than in the previous case, but the radiation is still confined to a narrow cone if $\omega_p/\omega\ll 1$.

The width of the radiation cone can be characterized in terms of the mean square angle of emission $\langle\theta^2\rangle$, defined as

$$\langle\theta^2\rangle \frac{d\mathcal{E}}{d\omega} = \int_0^\infty \frac{d^2\mathcal{E}}{d\omega d\theta}\,\theta^2 d\theta, \tag{19}$$

where

$$\frac{d\mathcal{E}}{d\omega} = \int_0^\infty \frac{d^2\mathcal{E}}{d\omega d\theta}\,d\theta. \tag{20}$$

Note that we have taken advantage of the sharp cutoff in $d^2\mathcal{E}/d\omega d\theta$ to extend the integrations in Eqs. (19) and (20) over the entire interval $0 \leq \theta < \infty$ rather than the limited interval $0 \leq \theta \lesssim 1$ for which (17) was derived. The errors introduced by this approximation are negligible. The integrations in Eqs. (19) and (20) are elementary, and we find that

$$\langle\gamma^2\theta^2\rangle \frac{d\mathcal{E}}{d\omega} = \frac{2e^2}{\pi c}\left[2 + x^{-2} - 2(1+x^2)\ln(1+x^{-2})\right] \tag{21}$$

and

$$\frac{d\mathcal{E}}{d\omega} = \frac{2e^2}{\pi c}\left[(2x^2+1)\ln(1+x^{-2}) - 2\right], \tag{22}$$

where x is the dimensionless parameter

$$x = \omega/\gamma\omega_p. \tag{23}$$

As would be expected from our earlier remarks, the quantity $\langle\gamma^2\theta^2\rangle$ approaches a constant limiting value for $x \gg 1$ ($\omega_p/\omega \ll \gamma^{-1}$),

$$\langle\gamma^2\theta^2\rangle \to 2, \quad x \gg 1 \tag{24}$$

and grows rapidly for x small ($\omega_p/\omega \gg \gamma^{-1}$),

$$\langle\gamma^2\theta^2\rangle \to [x^2 \ln x^{-2}]^{-1}, \quad x \ll 1. \tag{25}$$

It will be advantageous for our purposes to take the frequency dependence of $\langle\theta^2\rangle$ into account approximately, and consider instead of $\langle\gamma^2\theta^2\rangle$ a quantity $\langle\bar{\gamma}^2\theta^2\rangle$, with $\bar{\gamma}^2$ defined as

$$\frac{1}{\bar{\gamma}^2} = \frac{1}{\gamma^2} + \frac{\omega_p^2}{\omega^2} = \frac{1}{\gamma^2}\left(1 + \frac{1}{x^2}\right). \tag{26}$$

The variation of $\langle\gamma^2\theta^2\rangle^{1/2}$ and $\langle\bar{\gamma}^2\theta^2\rangle^{1/2}$ with x is shown in curves a and b in Fig. 1. The rapid approach of both quantities to their common limiting value, $\sqrt{2}$, is clearly evident. Note that $\langle\bar{\gamma}^2\theta^2\rangle^{1/2}$ approaches this limit from below, $\langle\bar{\gamma}^2\theta^2\rangle^{1/2} \leq \sqrt{2}$ for all x, a fact which we can use to obtain a useful upper bound on the root-mean-square angle of emission of the radiation at frequency ω,

$$\langle\theta^2\rangle^{1/2} \leq \bar{\theta} = \sqrt{2}\left(\frac{1}{\gamma^2} + \frac{\omega_p^2}{\omega^2}\right)^{1/2}. \tag{27}$$

This angle is quite small under the conditions of practical interest (for example, with $\gamma = 1000$, $\hbar\omega = 3$ keV, and $\hbar\omega_p = 30$ eV, $\bar{\theta} = 0.014$ rad $= 0.8°$).

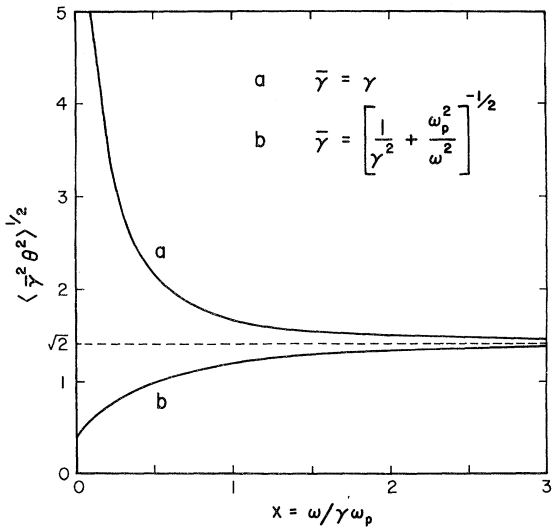

FIG. 1. Variation of the mean square angle of emission of the transition radiation from a thick slab as a function of the parameter $x = \omega/\gamma\omega_p$. Note the rapid approach of curves a and b to the limiting value $\sqrt{2}$ for x large.

The sharp forward peaking of the radiation is also evident from Fig. 2 in which we have plotted $\mathcal{F}(\theta < \theta_0)$, the fraction of the radiation emitted at angles θ less than a specified value θ_0, as a function of $\theta_0/\bar{\theta}$ for a number of values of x. The results for values of x greater than 10 are indistin-

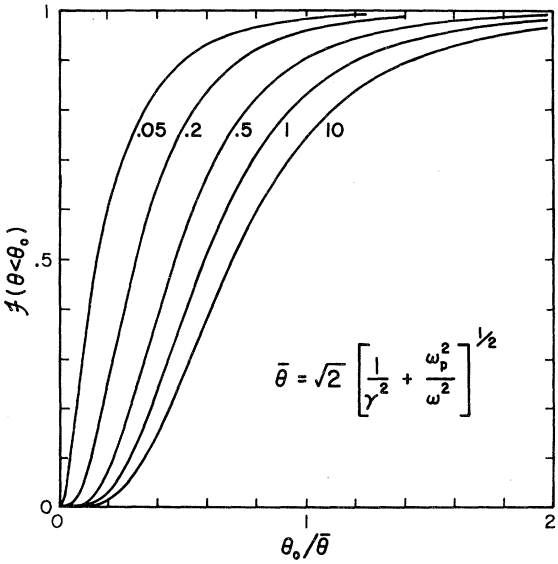

FIG. 2. The fraction of the transition radiation emitted at angles θ smaller than a given angle θ_0 as a function of $\theta/\bar{\theta}$ for various values of $x = \omega/\gamma\omega_p$. The curves for values of x larger than 10 are indistinguishable on the scale of the figure from that for $x = 10$.

guishable on the scale of the figure from the curve labeled $x = 10$. Even for this asymptotic curve, 74% of the radiation is emitted at angles smaller than $\bar{\theta}$, and 96% is emitted at angles less than $2\bar{\theta}$. These fractions are considerably higher for the values of x of principal interest, $x \ll 1$. The fraction $\mathcal{F}(\theta < \theta_0)$ can be calculated analytically:

$$\mathcal{F}(\theta < \theta_0) \frac{d\mathcal{E}}{d\omega} = \frac{d\mathcal{E}}{d\omega}(\theta < \theta_0),$$

where

$$\frac{d\mathcal{E}}{d\omega}(\theta < \theta_0) = \int_0^{\theta_0} \frac{d^2\mathcal{E}}{d\omega d\theta} d\theta = \frac{2e^2}{\pi c}\left[(2x^2+1)\ln\frac{(1+x^2)(1+y)^2}{1+x^2+x^2y^2} - \frac{x^2y^2}{1+x^2+x^2y^2} - \frac{y^2}{1+y^2}\right], \tag{28}$$

and

$$y^2 = \gamma^2\theta_0^2.$$

$d\mathcal{E}/d\omega$ is given by Eq. (22).

It is clear from Figs. 1(a) and 2 and Eq. (27) that the effective width of the radiation cone in an actual experiment will be determined by the minimum frequency ω_0 accepted by the apparatus. This frequency must be large relative to the plasma frequency ω_p if our approximations are to be valid. We assume that this is the case. If, in addition, $\gamma \gg \omega_0/\omega_p$, the radiation of all frequencies $\omega > \omega_0$ is confined to the interior of a cone with an opening angle $\theta \sim 2^{1/2}(\omega_p/\omega_0)$, with the higher-frequency radiation concentrated at smaller angles. The angular distribution of the radiation integrated over the frequency spectrum can be calculated using the spectrum in Eq. (17) weighted by the experimental frequency acceptance function. For purposes of illustration, we will consider the result obtained using a sharp lower cutoff ω_0,

$$\frac{d\mathcal{E}}{d\theta}(\omega > \omega_0) = \frac{e^2\omega_p}{c}\frac{\theta^3}{[\theta^2 + (1/\gamma^2)]^{5/2}} \times\left[1 - \frac{2}{\pi}\tan^{-1}\frac{\omega_0}{\omega_c} - \frac{2}{\pi}\frac{(\omega_0/\omega_c)}{1+(\omega_0/\omega_c)^2}\right]. \tag{29}$$

Here ω_c is a characteristic frequency given by

$$\omega_c = \omega_p[\theta^2 + (1/\gamma^2)]^{-1/2}. \tag{30}$$

The function $d\mathcal{E}(\omega > \omega_0)/d\theta$ is sharply peaked at small angles with a maximum at $\theta^2 \sim \frac{5}{2}\gamma^{-2}$, decreases as θ^{-2} out to $\theta \sim \omega_p/\omega_0$ ($\omega_0 \sim \omega_c$), and is cut off as θ^{-5} at larger angles (that is, for $\omega_0 > \omega_c$). The mean square angle of emission is easily estimated by using only the first term in Eq. (29) to calculate $\langle\theta^2\rangle$ and the total energy radiated, with θ restricted to the range $0 \leq \theta \leq \omega_p/\omega_0$. The result $\langle\theta^2\rangle_{\omega>\omega_0} \sim (\omega_p/\gamma\omega_0)$ agrees quite well with the result of an exact but lengthy calculation,

$$\langle\theta^2\rangle_{\omega>\omega_0} \sim \frac{3}{\pi}\frac{\omega_p}{\gamma\omega_0}, \quad \gamma \gg 1. \tag{31}$$

The angular distribution is consequently much broader than is often quoted,

$$\langle\theta^2\rangle^{1/2} \sim \gamma^{-1}(\gamma\omega_p/\omega_0)^{1/2} \gg \gamma^{-1} \text{ for } \gamma\omega_p/\omega_0 \gg 1,$$

but most of the energy is still radiated at quite small angles.

C. Frequency distribution of the radiation from a thick slab

The frequency spectrum of the transition radiation from a thick slab is quite simple when considered at a fixed angle $\theta \ll 1$. We find from Eq. (17) that

$$\left[\frac{d^2\mathcal{E}}{d\omega d\theta}(\omega, \theta)\right] \Big/ \left[\frac{d^2\mathcal{E}}{d\omega d\theta}(0, \theta)\right] = \left(1 + \frac{\omega^2}{\omega_c^2}\right)^{-2}, \tag{32}$$

where the cutoff frequency ω_c was defined in Eq. (30). The frequency distribution function in Eq. (32) decreases rapidly with increasing ω,[15] and the spectral intensity of the radiation becomes quite small for angular frequencies much above ω_c (see Fig. 3, curve a). Note, however, that $\omega_c \gg \omega_p$ if θ and γ^{-1} are sufficiently small. The fraction of the radiation emitted at frequencies ω less than a specified frequency $\omega_0 \gg \omega_p$ is easily calculated from Eq. (29),[16]

$$\left[\frac{d\mathcal{E}}{d\theta}(\omega < \omega_0)\right] \Big/ \left(\frac{d\mathcal{E}}{d\theta}\right) = \frac{2}{\pi}\left[\tan^{-1}\frac{\omega_0}{\omega_c} + \frac{\omega_0/\omega_c}{1+(\omega_0/\omega_c)^2}\right], \quad \omega_0, \omega_c \gg \omega_p. \tag{33}$$

This function is plotted in Fig. 3, curve b. Although 96% of the total energy is radiated at frequencies $\omega < 2\omega_c$, a significant fraction of the radiation may be at high frequencies if ω_c is sufficiently large.

The fixed-angle frequency spectrum is of less

interest in applications of transition radiation in high-energy physics than the spectrum obtained after integration of $d^2\mathcal{E}/d\omega d\theta$ over all angles of emission. The result obtained for the latter was noted in Eq. (22),

$$\frac{d\mathcal{E}}{d\omega} = \frac{2e^2}{\pi c} F(x), \tag{34}$$

where

$$F(x) = (2x^2+1)\ln(1+x^{-2}) - 2, \tag{35}$$

$x = \omega/\gamma\omega_p$, $x > \gamma^{-1}$. [The lower limit on x arises from the condition $\omega > \omega_p$ necessary for the validity of the high-frequency approximation for the dielectric function, Eq. (1), used throughout our discussion.] The function $F(x)$ is plotted in Fig. 4. Its behavior for small x is determined primarily by the logarithm in Eq. (35), $F(x) \sim (2\ln x^{-1} - 2)$, $\gamma^{-1} < x \ll 1$. $F(x)$ decreases rapidly with increasing x and varies asymptotically as x^{-4} (or ω^{-4}) for $x \gg 1$ as would be expected from Eq. (17),

$$F(x) \sim \frac{1}{6x^4} - \frac{1}{6x^6} + \frac{3}{20x^8} + O\left(\frac{1}{x^{10}}\right), \quad x \gg 1. \tag{36}$$

The total energy radiated at angular frequencies ω greater than some $\omega_0 > \omega_p$ is easily calculated from Eq. (34),

$$\mathcal{E}(\omega > \omega_0) = \frac{2}{\pi}\frac{e^2}{c}\gamma\omega_p\left[\tfrac{2}{3}\tan^{-1}\frac{1}{x_0} - x_0(\tfrac{2}{3}x_0^2+1)\ln\left(1+\frac{1}{x_0^2}\right) + \tfrac{2}{3}x_0\right], \tag{37}$$

$x_0 = \omega_0/\gamma\omega_p$. For fixed ω_0, x_0 decreases with increasing γ, and $\mathcal{E}(\omega > \omega_0)$ approaches an asymptotic form obtained by taking the small-x_0 limit of Eq. (37),

$$\mathcal{E}(\omega > \omega_0) \sim \frac{2}{3}\frac{e^2}{c}\gamma\omega_p\left[1 - \frac{6x_0}{\pi}\ln\frac{1}{x_0} + O(x_0^3)\right], \quad x_0 \ll 1 \tag{38}$$

$$= \frac{2}{3}\frac{e^2}{c}\left[\gamma\omega_p - \frac{6\omega_0}{\pi}\ln\frac{\gamma\omega_p}{\omega_0} + O\left(\frac{1}{\gamma^2}\right)\right]. \tag{39}$$

The leading term in Eq. (38) is generally quoted as giving the total energy radiated by an ultrarelativistic particle in traversing a thick dielectric slab,[2]

$$\mathcal{E} = \frac{2}{3}\frac{e^2}{c}\gamma\omega_p = 1.46\times10^{-4}\gamma \text{ keV}, \quad \hbar\omega_p = 30 \text{ eV}. \tag{40}$$

However, it should be noted that the absolute error in $\mathcal{E}(\omega > \omega_0)$ which results from the omission of the second term in Eq. (39) increases logarithmically with γ, even though the fractional error decreases with increasing γ [decreasing x_0, Eq. (38)]. This effect is evident in Fig. 5 which shows the dependence of $\mathcal{E}(\omega > \omega_0)$ on γ for several values of

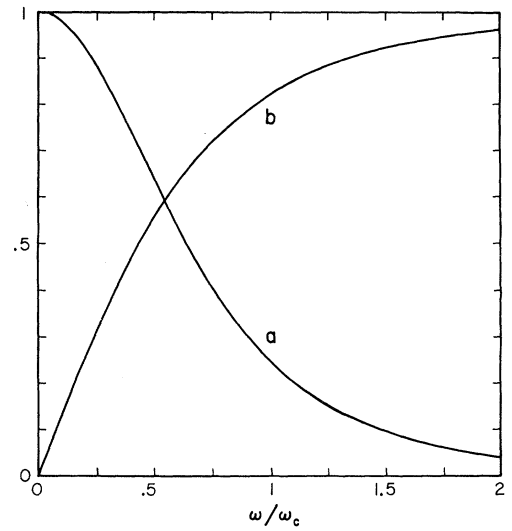

FIG. 3. (a) The frequency spectrum of the transition radiation at a fixed angle θ, $[d^2\mathcal{E}(\omega, \theta)/d\omega d\Omega]/[d^2\mathcal{E}(0, \theta)/d\omega d\Omega]$, as a function of ω/ω_c. The cutoff frequency ω_c is given by $\omega_c = \omega_p[\theta^2 + (1/\gamma^2)]^{-1/2}$. (b) The fraction of the energy emitted at a fixed angle at frequencies less than a given frequency ω as a function of ω/ω_c.

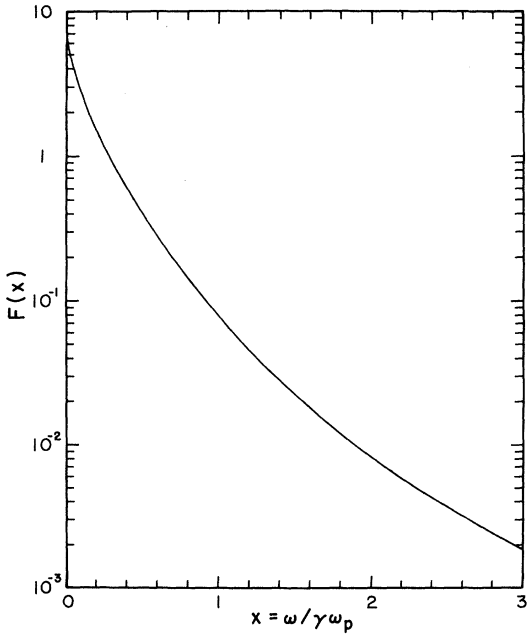

FIG. 4. Variation of the spectral distribution function $F(x)$, Eq. (35), with the parameter $x = \omega/\gamma\omega_p$. The frequency spectrum of the transition radiation from a thick slab is given by $d\mathcal{E}/d\omega = (2e^2/\pi c)F(x)$.

ω_0. The curve labeled $\hbar\omega_0 = 0$ gives the result calculated from Eq. (40). This result is unphysical, since our calculations are only valid if $\omega_0 > \omega_p$.

The possibility of using transition radiation to measure the energy of, or discriminate among, ultrarelativistic charged particles depends on the rapid increase in $\mathcal{E}(\omega > \omega_0)$ with γ, and the fact that the spectrum extends into the x-ray region to frequencies high enough that background problems can be reduced or eliminated (see, e.g., Ref. 3). The fraction of the total energy radiated at frequencies $\omega > \omega_0 \gg \omega_p$ is given to sufficient accuracy for our purposes by the ratio $\mathcal{E}(\omega > \omega_0)/\mathcal{E}$, Eqs. (37) and (40). This quantity is plotted in Fig. 6 as a function of $x_0 = \omega_0/\gamma\omega_p$. The ratio decreases rapidly with increasing x_0 and falls asymptotically as x_0^{-3} for $x_0 \gg 1$,

$$\frac{\mathcal{E}(\omega > \omega_0)}{\mathcal{E}} \sim \frac{1}{6\pi}\frac{1}{x_0^3}\left[1 - \frac{3}{5}\frac{1}{x_0^2} + O\left(\frac{1}{x_0^4}\right)\right], \quad x_0 \gg 1 . \tag{41}$$

Despite this rapid decrease, a substantial fraction of the radiation will be in the x-ray region if γ is sufficiently large. For example, 56% of the energy is radiated at frequencies with $\hbar\omega > 3$ keV for $\hbar\omega_p = 30$ eV and $\gamma > 1000$. The mean angular frequency of the radiation is also easily calculated from Eq. (34),

$$\bar{\omega} \sim \frac{3}{4\pi}\gamma\omega_p[1 + O(\gamma^{-1})], \quad \gamma \gg 1 . \tag{42}$$

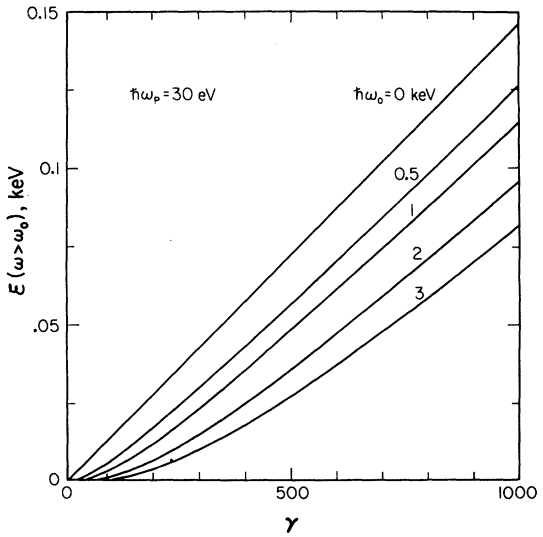

FIG. 5. The energy $\mathcal{E}(\omega > \omega_0)$, Eq. (37), radiated at frequencies $\omega > \omega_0$ as a function of γ for a plasma energy $\hbar\omega_p = 30$ eV and various values of ω_0. The curve for $\hbar\omega_0 = 0$ gives the total energy radiated by a thick slab, neglecting the corrections necessary for $\omega_0 < \omega_p$, $\mathcal{E} = (2e^2/3c)\gamma\omega_p$.

For $\gamma > 420$, $\hbar\bar{\omega}$ is greater than 3 keV. These results will be altered in detail for real devices. However, the analog of Eq. (37) can be calculated by weighting the spectral intensity function $d\mathcal{E}/d\omega$, Eq. (34), by the frequency acceptance function for the device and integrating over ω. The result will determine the relation between the energy detected and γ for the device in question. The examples given above correspond to an ideal detector which accepts all radiation with $\omega > \omega_0$ and no radiation of lower frequency.

D. Photon number distributions

The number of photons per unit frequency emitted in transition radiation from a single slab is given by

$$\frac{dN}{d\omega} = \frac{1}{\hbar\omega}\frac{d\mathcal{E}}{d\omega} = \frac{2\alpha}{\pi}\frac{1}{\gamma\omega_p}\frac{1}{x}F(x), \quad x = \omega/\gamma\omega_p \tag{43}$$

where $\alpha \approx \frac{1}{137}$ is the fine-structure constant. The function $F(x)$ is defined in Eq. (35) and is graphed in Fig. 4. The number of photons emitted at frequencies above some minimum frequency ω_0 is easily obtained by integrating Eq. (43) from ω_0 to ∞,

$$N(\omega > \omega_0) = (\alpha/\pi)[2 - 2(x_0^2 + 1)\ln(1 + x_0^{-2}) - f(1 + x_0^{-2})] . \tag{44}$$

Here $f(z)$ is the Spence function (Euler dilogarithm)[17] defined by the integral

$$f(z) = -\int_1^z \frac{\ln t}{t - 1}\,dt . \tag{45}$$

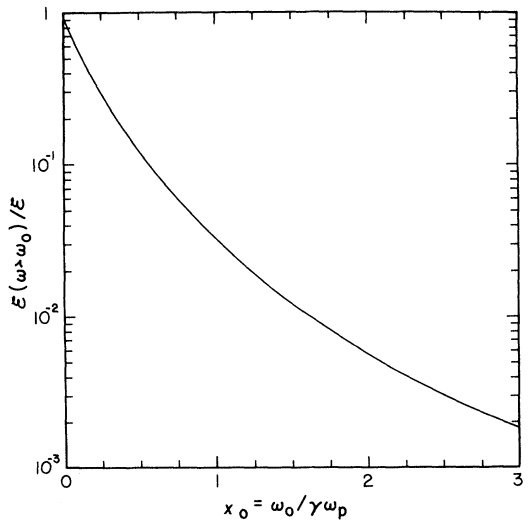

FIG. 6. The fraction of the total energy radiated at frequencies $\omega > \omega_0$ as a function of $x_0 = \omega_0/\gamma\omega_p$.

$N(\omega > \omega_0)$ is plotted in Fig. 7 as a function of $x_0 = \omega_0/\gamma\omega_p$. This number is extremely small for large values of x_0 and should properly be interpreted as the average number of photons with $\omega > \omega_0$ which will be obtained in a set of independent measurements. The probability of finding n photons in a set of measurements is given by a Poisson distribution with $\bar{n} = N$.

The function $N(\omega > \omega_0)$ is replotted in Fig. 8 as a function of γ for various values of the minimum frequency ω_0, and our standard value of the plasma energy, $\hbar\omega_p = 30$ eV. It is evident from this figure that a transition radiation detector with a minimum acceptance energy of ~3 keV would be very insensitive in terms of the number of photons detected to particles with $\gamma \lesssim 200$–300. The number of photons above 3 keV continues to increase slowly with γ for $\gamma > 300$, but the increase is not rapid enough for absolute measurements of $N(\omega > \omega_0)$ to be useful as a way of measuring γ. However, it is possible that one could use the sharp initial rise in $N(\omega > \omega_0)$ with γ for an appropriate choice of ω_0 to construct a "threshold" transition radiation detector sensitive, for example, to pions but not to protons. Thus, for $\hbar\omega_0 = 3$ keV, the average counting rate of such a detector would be roughly 36 times as high for 140-GeV pions as for 140-GeV protons.

While the number of photons emitted at frequencies $\omega > \omega_0$ increases only slowly with γ for large values of γ, the average energy carried by each photon, hence, the total energy radiated in this spectral region, increases nearly linearly with γ [see Eq. (39) and Fig. 5]. It therefore appears to be more practical to operate transition radiation detectors in a mode in which the total energy $\mathcal{E}(\omega > \omega_0)$ is measured than to rely on photon counting rates. Either direct measurements of the γ values of different particles or a threshold type of particle discrimination would appear to be possible in principle in this mode. The quantity $\mathcal{E}(\omega > \omega_0)$ is again to be interpreted statistically, as the average value of the energy radiated at frequencies $\omega > \omega_0$ which will be found in a set of independent measurements, with the photon numbers satisfying a Poisson distribution.

E. The formation zone effect

We will return at this point to the discussion of the complete expression for the transition radiation from a slab, Eq. (16), and in particular, of the validity of the approximation made in going from Eq. (16) to Eq. (17). Our approximation consisted of dropping the cosine in the last factor in our expression for $d^2\mathcal{E}/d\omega d\theta$,

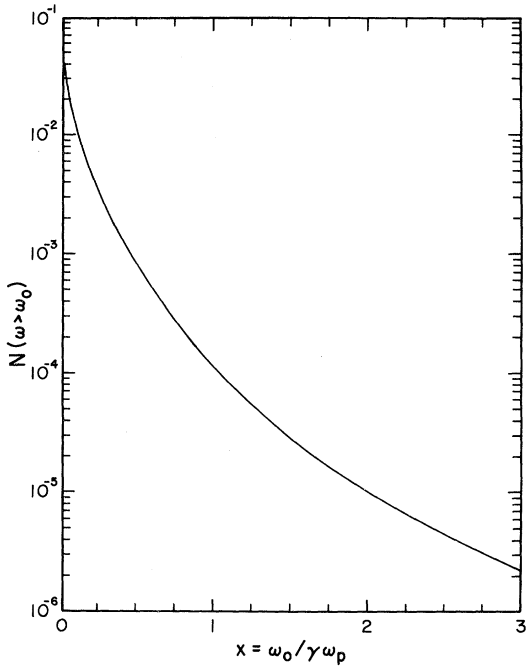

FIG. 7. The number of photons radiated at frequencies $\omega > \omega_0$ by a single particle traversing a thick dielectric slab as a function of $x_0 = \omega_0/\gamma\omega_p$.

$$\frac{d^2\mathcal{E}}{d\omega d\theta} = \frac{4e^2}{\pi c}\left(\frac{\omega_p}{\omega}\right)^4 \frac{\theta^3}{[\theta^2 + (1/\gamma^2)]^2[\theta^2 + (1/\gamma^2) + (\omega_p^2/\omega^2)]^2} \times \left[1 - \cos\left(\frac{\omega}{v} - \kappa_z\right) a\right] . \quad (46)$$

The argument of the cosine is essentially the ratio

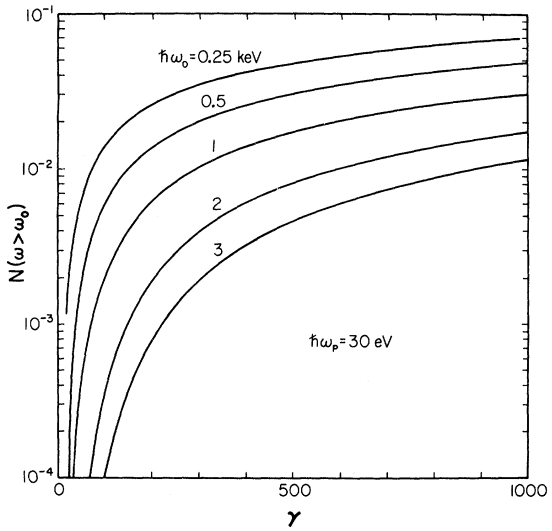

FIG. 8. The number of photons radiated at frequencies $\omega > \omega_0$ as a function of γ for a plasma energy $\hbar\omega_p = 30$ eV, and various choices of $\hbar\omega_0$.

of the thickness of the slab to the separation Λ between points in the slab which radiate in phase,

$$\left(\frac{\omega}{v}-\kappa_z\right)a=\frac{2\pi a}{\Lambda}\,, \tag{47}$$

where

$$\Lambda(\theta,\gamma,\omega)=2\pi\left(\frac{\omega}{v}-\kappa_z\right)^{-1} \sim\frac{4\pi c}{\omega}\left(\theta^2+\frac{1}{\gamma^2}+\frac{\omega_p^2}{\omega^2}\right)^{-1}. \tag{48}$$

The appearance of this finite coherence length is a reflection of the difference between the phase velocities of the radiation field and the electric field of the particle, Eq. (5). Because of this difference, radiation fields which originate at different depths in the slab, with phases determined by the local phase of the electric field of the particle, will differ in phase at the point of observation and may interfere either constructively or destructively. The last factor in Eq. (46) describes this interference.

The quantity $\Lambda_0/2\pi=\Lambda(0,\gamma,\omega)/2\pi$ is generally described in the literature as the depth of the "formation zone" in which the radiation field builds up to a reasonable fraction of its maximum possible value. This interpretation follows from consideration of the radiation emitted by a thin foil. In particular, if a is small enough for given values of ω, γ, and θ that $2\pi a/\Lambda<1$, we may approximate the cosine in Eq. (46) by the first two terms in its Taylor series, and find that $d^2\mathcal{E}/d\omega d\theta$ increases as a^2,

$$\frac{d^2\mathcal{E}}{d\omega d\theta}\to\frac{e^2}{2\pi c}\left(\frac{\omega_p}{\omega}\right)^2\left(\frac{\omega_p a}{c}\right)^2\frac{\theta^3}{[\theta^2+(1/\gamma^2)]^2}\,,$$

$$2\pi a/\Lambda<1\,. \tag{49}$$

This quadratic increase in the energy radiated corresponds to a linear increase in the strength of the electric field with the thickness of the foil, precisely the result which would be expected for a coherent radiator.

The importance of the interference terms in Eq. (46) for practical transition radiation detectors depends on thickness (and separation) of the foils used and on the ranges of angles and frequency accepted by the device. In the following discussion, we will assume that $\gamma\gg1$, $\omega/\omega_p\gg1$, and $(\omega_p a/c)\gg1$ ($c/\omega_p=0.66\times10^{-6}$ cm for $\hbar\omega_p=30$ eV). Under these conditions, our earlier conclusion that the radiation is confined to a narrow cone around the direction of motion of the particle is unchanged, though the details of the angular distribution are modified. These modifications are not of importance for practical devices, and we will consider only the spectrum of the radiation obtained when all angles of emission are accepted. The angular integration necessary to obtain $d\mathcal{E}/d\omega$ from Eq. (46) can be performed exactly in terms of the sine- and cosine-integral functions[18]

$$\frac{d\mathcal{E}}{d\omega}=\frac{2e^2}{\pi c}[F(x)+G(\tau,x)]\,, \tag{50}$$

where $x=\omega/\gamma\omega_p$, $\tau=(\omega_p a/2\gamma c)$, and

$$G(\tau,x)=-(2x^2+1)[\mathrm{Ci}(\tau(x+x^{-1}))-\cos(\tau/x)\,\mathrm{Ci}(\tau x)+\sin(\tau/x)\,\mathrm{si}(\tau x)]+2\cos(\tau(x+x^{-1})) +\tau(x+x^{-1})\,\mathrm{si}(\tau(x+x^{-1}))+\tau x\cos(\tau/x)\,\mathrm{si}(\tau x)+\tau x\sin(\tau/x)\,\mathrm{Ci}(\tau x)\,. \tag{51}$$

The function $F(x)$ is defined in Eq. (35).

Simple limiting expressions for $d\mathcal{E}/d\omega$ can be obtained for the cases of very thin or very thick foils directly from Eq. (50), or by making the relevant approximations in Eq. (46) before performing the angular integration. We will call a foil "thin" if its thickness a is small compared to the length of the formation zone, $2\pi a/\Lambda_0\ll1$. This condition requires that $\omega_p(\omega_p a/2c)\lesssim\omega\lesssim2\gamma^2c/a$. The argument of the cosine in Eq. (46) is then small for angles in the range $0\leq\theta\lesssim(2c/\omega a)^{1/2}$, and the radiation in this angular region is strongly suppressed. The angular distribution of the radiation is given by Eq. (49) for $\theta<(2c/\omega a)^{1/2}$, and is sharply cut off at larger angles. While this distribution is broader than that considered in Sec. II B, but is still quite narrow at high frequencies, $1\gg(2c/\omega a)^{1/2}\gg\bar{\theta}$ [see Eq. (27)]. We can obtain an approximate expression for the frequency spectrum of the radiation from a thin foil by integrating Eq. (49) over the angular interval $0\leq\theta\leq(2c/\omega a)^{1/2}$,

$$\frac{d\mathcal{E}}{d\omega}\approx\frac{e^2}{4\pi c}\left(\frac{\omega_p}{\omega}\right)^2\left(\frac{\omega_p a}{c}\right)^2\left(\ln\frac{2\gamma^2c}{\omega a}-C\right),$$

$$2\gamma^2c/a\gg\omega\gg\omega_p(\omega_p a/2c)\,. \tag{52}$$

Here C is a constant on the order of 1. The spectrum falls to a reasonable approximation as ω^{-2} in the region to which Eq. (51) is applicable. The total energy radiated at frequencies $\omega>\omega_0$ is given approximately by

$$\mathcal{S}(\omega > \omega_0) \approx \frac{e^2}{4\pi c}\,\omega_p \left(\frac{\omega_p}{\omega_0}\right)\left(\frac{\omega_p a}{c}\right)^2 \left(\ln\frac{2\gamma^2 c}{\omega_0 a} - C'\right),$$

$$2\gamma^2 c/a \gg \omega \gg \omega_p(\omega_p a/2c). \quad (53)$$

This quantity increases much less rapidly with increasing γ than the result for an infinitely thick slab given in Eq. (39), and the intensity of the radiation is strongly suppressed.

The limiting case of "very thick" foils is also easily discussed. This limit is defined by the condition that the cosine in Eq. (46) undergo many oscillations in the smallest angular interval in which the remaining factors in Eq. (46) vary significantly. We would then expect the contribution of the cosine term to $d\mathcal{S}/d\omega$ to be quite small because of large cancellations in the angular integration. Since the leading factors in Eq. (46) vary rapidly for $0 \leq \theta \lesssim \gamma^{-1}$ and less rapidly for larger θ, the foregoing condition on the oscillations of the cosine requires that $(\omega a/2\gamma^2 c) \gg 1$ at the frequencies of interest. It is straightforward in this case using repeated partial integrations to obtain an asymptotic expansion for the contributions to $d\mathcal{S}/d\omega$ associated with the cosine term in Eq. (46), hence, to obtain an asymptotic expansion for the frequency spectrum of the radiation,

$$\frac{d\mathcal{S}}{d\omega} = \frac{2e^2}{\pi c}\{F(x) + (\tau x)^{-2}(1+x^2)^{-2}[\cos\tau(x+x^{-1}) - 2((\tau x)^{-2} + \tau^{-2}(x+x^{-1})^{-2})\sin\tau(x+x^{-1}) + \cdots]\}, \quad (54)$$

where $F(x)$ is defined in Eq. (35), $\tau = (\omega_p a/2\gamma c)$, and $x = \omega/\gamma\omega_p$. This result approaches that for the infinitely thick slab, Eq. (34), for $\tau \to \infty$.

Neither of the foregoing limits is applicable to practical transition counters of the types which have been constructed.[3,4] In particular, the very weak dependence of the energy radiated by a "thin" foil on γ, in conjuction with strong suppression of the intensity of the radiation, makes thin-foil counters impractical. The foil thicknesses used in present counters [$a \sim 1\text{-}2.5\times10^{-3}$ cm (see Refs. 3 and 4)] are consequently well above the "thin" limit. (Note that a foil will not be "thin" at any frequency if $a > \gamma c/\omega_p \sim 0.66\gamma\times10^{-6}$ cm, a condition which follows from the use of the maximum value of Λ_0 in the thin-foil condition $2\pi a/\Lambda_0 < 1$.) On the other hand, the amount of material in the way of a particle beam, hence the probability of unwanted interactions in the counter, becomes unacceptably large if the foils are to be "very thick" for large γ. The foil thicknesses noted above are acceptable in this respect, but fail to satisfy the "very thick" foil constraint $a \gg (2\gamma^2 c/\omega)$ for reasonable values of $\hbar\omega$ and γ larger than a few hundred. We are therefore forced in the case of practical counters to deal with the rather complicated result for $d\mathcal{S}/d\omega$ given in Eq. (50).

The first term in Eq. (50) describes the transition radiation from an infinitely thick slab. The effect of finite slab thickness on $d\mathcal{S}/d\omega$ is described by the function $G(\tau, x)$. It is simple to obtain a bound on $|G(\tau, x)|$ by replacing the cosine in Eq. (46) by its extreme values, ± 1, before performing the angular integration. One finds that

$$|G(\tau, x)| \leq F(x). \quad (55)$$

However, this bound is substantially too weak under the conditions of primary interest. Most of the radiation is emitted at frequencies $\omega \ll \gamma\omega_p$ ($x \ll 1$) and at angles $\theta \lesssim \theta_{\max}$, where

$$\theta_{\max}^2 \gtrsim \frac{1}{\gamma^2} + \frac{\omega_p^2}{\omega^2}.$$

Since $(\omega a/2c)\theta_{\max}^2 = \tau(x + x^{-1})$, the cosine in Eq. (46) will undergo many oscillations in the region of integration if $\tau > 1$ and $x \ll 1$. The resulting cancellations reduce the magnitude of $G(\tau, x)$ well below the absolute bound in Eq. (55).

$G(\tau, x)$ also oscillates rapidly as a function of x or ω. This property of $G(\tau, x)$ can be displayed by reexpressing the sin- and cosine-integral functions in Eq. (51) in terms of auxiliary functions $f(z)$ and $g(z)$ defined by[18]

$$f(z) = \mathrm{Ci}(z)\sin z - \mathrm{si}(z)\cos z = \int_0^\infty \frac{1}{t^2+1}\,e^{-zt}\,dt, \quad (56)$$

$$g(z) = -\mathrm{Ci}(z)\cos z - \mathrm{si}(z)\sin z = \int_0^\infty \frac{1}{t^2+1}\,e^{-zt}\,dt. \quad (57)$$

These functions clearly decrease monotonically with increasing z, with $f(z) \sim z^{-1}$ and $g(z) \sim z^{-2}$ for $z \to \infty$. For $z \to 0$, $f(z) \to \pi/2$, while $g(z)$ diverges logarithmically, $g(z) \sim \ln z^{-1}$. $G(\tau, x)$ can be expressed in terms of these functions as

$$G(\tau, x) = \cos(\tau(x+x^{-1}))\{(2x^2+1)[g(\tau(x+x^{-1})) - g(\tau x)] - \tau(x+x^{-1})f(\tau(x+x^{-1})) - \tau x f(\tau x) + 2\}$$
$$+ \sin(\tau(x+x^{-1}))\{(2x^2+1)[f(\tau x) - f(\tau(x+x^{-1}))] - \tau(x+x^{-1})g(\tau(x+x^{-1})) - \tau x g(\tau x)\}. \quad (58)$$

The factors in curly brackets vary smoothly as functions of x or ω, while the sine and cosine functions oscillate rapidly with ω for $\tau > 1$ and $x \ll 1$.[19] As a result, there will be large cancellations when $G(\tau, x)$ is integrated or averaged over a range of frequencies broad enough to include many oscillations. This requires that the change in $\tau(x + x^{-1})$ over the frequency band be large, $\Delta(\tau(x + x^{-1}))/2\pi \gg 1$. The net contribution of the thickness-dependent terms to the total energy radiated is then small compared to the contribution of the thickness-independent term $F(x)$. We conclude that the approximation of using the simple result for $d\mathcal{E}/d\omega$ given in Eq. (34) to describe the radiation from a broad-band transition counter at frequencies $\omega \ll \gamma\omega_p$ should be adequate for most practical purposes provided that $(\omega_p a/2\gamma c) > 1$.

F. Absorption of radiation in the slab

We have so far neglected any absorption of the transition radiation in the dielectric slab. This absorption can be quite important for soft x-rays even for the thin plastic foils used in current experiments (typically Mylar foils $1 - 2.5 \times 10^{-3}$ cm thick[3,4]). Thus, the x-ray absorption length in polypropylene is 0.64×10^{-3} cm at 1 keV, 1.1×10^{-3} cm at 1.25 keV, 4.2×10^{-3} cm at 2 keV, 1.5×10^{-2} cm at 3 keV, 1.2×10^{-1} cm at 6 keV, and 0.5 cm at 10 keV.[20] The absorption lengths in Mylar are smaller by factors of 0.65 to 0.57 over this energy range. It is clear from these numbers that transition radiation in the 1–2 keV range will be strongly absorbed in the foil in which it is emitted, and that radiation of higher energy may also undergo significant absorption in traversing later foils in a multifoil stack.[21]

The effects of absorption in a single foil are described to sufficient accuracy for our purposes by making the replacement

$$e^{-i\vec{\kappa}\cdot\vec{r}} \to e^{-i\vec{\kappa}\cdot\vec{r} + \lambda z/(2\cos\theta)} \tag{59}$$

in Eq. (13a), where $\lambda(\omega)$ is the x-ray energy absorption coefficient for the material in question. The extra factor describes the attenuation of the transition radiation emitted inside the foil ($-a < z < 0$) during its propagation to the surface. The result for the asymptotic vector potential in Eq. (13b) is modified accordingly:

$$\vec{A}(\vec{r}', \omega) \underset{r' \to \infty}{\sim} \frac{i}{(2\pi)^{1/2}} \frac{e}{v} \frac{\omega}{c} \frac{\epsilon - 1}{(\omega/v) - \kappa_z - i\lambda/(2\cos\theta)} \times \frac{\vec{\kappa}_\perp}{\kappa_\perp^2 + (\omega/\gamma v)^2} \times \left[1 - e^{i(\kappa_z - \omega/v)a - \lambda a/(2\cos\theta)}\right] \frac{e^{ikr'}}{r'} . \tag{60}$$

For foils composed primarily of light elements, $\lambda/(2\cos\theta)$ is small compared to $[(\omega/v) - \kappa_z]$ at all frequencies $\omega \gg \omega_p$ for θ small,

$$\frac{\omega}{v} - \kappa_z > \frac{\omega_p}{2c} \frac{\omega_p}{\omega} \gg \tfrac{1}{2}\lambda(\omega), \quad \omega \gg \omega_p \tag{61}$$

and can be dropped in the denominator in Eq. (60). The quantities $d^2\mathcal{E}/d\omega d\Omega$ and $d\mathcal{E}/d\omega$ are then given in the usual high-energy, high-frequency, small-angle limit by

$$\frac{d^2\mathcal{E}}{d\omega d\Omega} \sim \frac{e^2}{\pi^2 c} \left(\frac{\omega_p}{\omega}\right)^4 \times \frac{\theta^2}{[\theta^2 + (1/\gamma^2) + (\omega_p^2/\omega^2)][\theta^2 + (1/\gamma^2)]^2} \times \left[1 + e^{-\lambda a} - 2e^{-(\lambda/2)a} \cos\left(\frac{\omega}{v} - \kappa_z\right) a\right], \quad \gamma \gg 1, \ \omega \gg \omega_p, \ \theta \ll 1 \tag{62}$$

$$\frac{d\mathcal{E}}{d\omega} \sim \frac{e^2}{\pi c}\left[(1 + e^{-\lambda a}) F(x) + 2e^{-(\lambda/2)a} G(\tau, x)\right] . \tag{63}$$

The functions $F(x)$ and $G(\tau, x)$ are defined in Eqs. (35) and (51). For optically thick foils, $\lambda a \gg 1$, these results for $d^2\mathcal{E}/d\omega d\Omega$ and $d\mathcal{E}/d\omega$ reduce to one half of the corresponding "thick-slab" results given in Eqs. (17) and (34).

III. GENERALIZATIONS FOR DIFFERENT GEOMETRIES

A. Oblique incidence on a single slab

The results of the preceding section were derived for the case of normal incidence of an ultrarelativistic charged particle on a dielectric slab. The discussion will be generalized in the present section to the case of oblique incidence. We will show, in particular, that the results derived for normal incidence can be used with minor modifications to describe an appropriate azimuthal average of the transition radiation emitted in the case of oblique incidence.[22]

It will be convenient in the ensuing calculations to use the two different coordinate systems shown in Fig. 9. The common origin of the two systems is at the point where the particle emerges from the slab. Ths system denoted by x, y, z has its z axis oriented perpendicular to the slab and its x axis in the plane determined by $\hat{z}$ and the velocity of the particle, $\vec{v}$. The x', y', z' system has the z' axis along $\vec{v}$ and the x' axis in the plane determined by $\vec{v}$ and $\hat{z}$, as indicated. We will specify the direction of the wave vector $\vec{k}$ for the radiation outside the slab by angles θ, ϕ referred to the x', y', z' system. The direction of $\vec{k}$ with respect to the x, y, z system will be specified by the angles Θ, Φ, and the direction of $\vec{v}$ in this system,

by the angles $\vartheta, 0$.

The basic calculation for the case of oblique incidence is quite similar to that for normal incidence given in Sec. IIA. We will again assume that the electric field in the slab is given by the vacuum field of the incident particle, and will neglect multiple reflections of the radiation field in the slab. The asymptotic form of the vector potential which describes the radiation field is given in this approximation by

$$\vec{A}(\vec{r}',\omega) \underset{r'\to\infty}{\sim} -i\,\frac{\omega}{c}\,\frac{\epsilon-1}{4\pi}\,\frac{e^{ikr'}}{r'}\int d^3r\, e^{-i\vec{K}\cdot\vec{r}}\,\vec{E}_{\rm vac}(\vec{r},\omega)$$
$$= -\frac{1}{(2\pi)^{1/2}}\,\frac{e}{\pi v}\,\frac{\omega}{c}\,\frac{\epsilon-1}{4\pi}\,\frac{e^{ikr'}}{r'}\int d^2q\,\frac{\vec{q}+(\omega/\gamma^2 v)\hat{v}}{q^2+(\omega/\gamma v)^2}\int_{-a}^{0}dz\int dx\,dy\,e^{-i\vec{K}\cdot\vec{r}+i\vec{q}\cdot\vec{r}+i(\omega/v)\hat{v}\cdot\hat{r}}, \tag{64}$$

where $\vec{K}$ is the wave vector of the radiation inside the slab. The relation of $\vec{K}$ to $\vec{k}$ is given in Eqs. (11), with θ replaced by Θ. The vector $\vec{q}$ in Eq. (64) is transverse relative to $\vec{v}$, $\vec{q}\cdot\hat{v}=q_{z'}=0$ [see Eqs. (6)].

The integral over the volume of the slab in Eq. (64) can be evaluated using the rectangular coordinates x, y, z, as indicated. The remaining integral over $\vec{q}$ can then be performed using the primed coordinate system. The result is rather complicated:

$$\vec{A}(\vec{r}',\omega) \underset{r'\to\infty}{\sim} \frac{i}{(2\pi)^{1/2}}\,\frac{e}{v}\,\frac{\omega}{c}\,(\epsilon-1)\,\frac{e^{ikr'}}{r'}\left\{\left[\kappa_{x'}-\left(\frac{\omega}{v}-\kappa_{z'}\right)\tan\vartheta\right]\hat{x}'+\kappa_{y'}\,\hat{y}'+\frac{\omega}{\gamma^2 v}\,\hat{z}'\right\}$$
$$\times\left[\kappa_{x'}^2+\kappa_{y'}^2+\left(\frac{\omega}{\gamma v}\right)^2-2\kappa_{x'}\left(\frac{\omega}{v}-\kappa_{z'}\right)\tan\vartheta+\left(\frac{\omega}{v}-\kappa_{z'}\right)^2\tan^2\vartheta\right]^{-1}\left(\frac{\omega}{v}-\kappa_{z'}\right)^{-1}\left[1-e^{i(\kappa_z-\omega/v)a/\cos\vartheta}\right]. \tag{65}$$

Note that the exponential involves the slant thickness of the slab $a/\cos\vartheta$, as would be expected. The expression for $\vec{A}$ vanishes for $\vartheta\to\pi/2$, corresponding to motion of the particle parallel to the surface of the slab. Our approximations are not appropriate in this case, and we will therefore restrict our attention to angles $\vartheta<\pi/2$.

Calculation of the energy radiated per unit solid angle per unit angular frequency is straightforward. For $\gamma\gg1$ and $\omega/\omega_p\gg1$, the radiation is sharply peaked at small angles θ relative to the direction of motion of the charged particle. It is therefore convenient to introduce a small-angle approximation as in our earlier calculations. Using the relations given in Eqs. (11) with θ replaced by Θ, and the geometry of Fig. 9, we find that

$$\kappa_{x'}=\frac{\omega}{c}\left[\sin\Theta\cos\vartheta\cos\Phi-(\epsilon-\sin^2\Theta)^{1/2}\sin\vartheta\right]\sim\frac{\omega}{c}\left(\sin\theta\cos\phi+\frac{1}{2}\,\frac{\omega_p^2}{\omega^2}\,\frac{\sin\vartheta}{\cos\Theta}+\cdots\right),\qquad \omega_p/\omega\ll\cos\Theta$$
$$\sim\frac{\omega}{c}\left(\theta\cos\phi+\frac{1}{2}\,\frac{\omega_p^2}{\omega^2}\tan\vartheta+\cdots\right),\qquad \theta\ll1;$$
$$\kappa_{y'}=\frac{\omega}{c}\sin\theta\sin\phi\sim\frac{\omega}{c}\,\theta\sin\phi,\qquad \theta\ll1; \tag{66}$$
$$\kappa_{z'}=\frac{\omega}{c}\left[\sin\Theta\sin\vartheta\cos\Phi+(\epsilon-\sin^2\Theta)^{1/2}\cos\vartheta\right]\sim\frac{\omega}{c}\left(\cos\theta-\frac{1}{2}\,\frac{\omega_p^2}{\omega^2}\,\frac{\cos\vartheta}{\cos\Theta}+\cdots\right),\qquad \omega_p/\omega\ll\cos\Theta$$
$$\sim\frac{\omega}{c}\left(1-\tfrac{1}{2}\theta^2-\frac{1}{2}\,\frac{\omega_p^2}{\omega^2}-\frac{\theta}{2}\,\frac{\omega_p^2}{\omega^2}\tan\vartheta\cos\phi+\cdots\right),\qquad \theta\ll1.$$

We have used the fact that $\cos\Theta\to\cos\vartheta$ for $\theta\ll1$ in the final forms of these expressions. With these approximations, we find that

$$\frac{d^2\mathcal{E}}{d\omega\,d\Omega}\sim\frac{2e^2}{\pi^2 c}\left(\frac{\omega_p}{\omega}\right)^4\left[\theta^2-\theta\left(\theta^2+\frac{1}{\gamma^2}\right)\tan\vartheta\cos\phi\right]$$
$$\times\left[\theta^2+\frac{1}{\gamma^2}-\theta\left(\theta^2+\frac{1}{\gamma^2}\right)\tan\vartheta\cos\phi\right]^{-2}\left(\theta^2+\frac{1}{\gamma^2}+\frac{\omega_p^2}{\omega^2}+\theta\,\frac{\omega_p^2}{\omega^2}\tan\vartheta\cos\phi\right)^{-2}$$
$$\times\left[1-\cos\frac{\omega a}{2c\cos\vartheta}\left(\theta^2+\frac{1}{\gamma^2}+\frac{\omega_p^2}{\omega^2}+\theta\,\frac{\omega_p^2}{\omega^2}\tan\vartheta\cos\phi\right)\right],\qquad \theta\tan\vartheta\ll1. \tag{67}$$

We have consistently dropped terms of fourth order in the small quantities θ, γ^{-1}, and ω_p/ω in various factors in Eq. (67), and have retained third-order terms only to indicate the weak dependence of the radiation on the azimuthal angle ϕ.

The restriction $\theta\tan\vartheta \ll 1$ necessary for our approximations to be valid is essentially the condition that the radiation cone not intersect the plane of the slab.[23] We will assume that ϑ, ω, and γ are such that this condition is satisfied with θ replaced by $2\bar{\theta}$, where $\bar{\theta}$ is the upper bound on the root-mean-square angle of emission defined in Eq. (27),

$$2\bar{\theta}\tan\vartheta \ll 1, \quad \bar{\theta} = \sqrt{2}\left(\frac{1}{\gamma^2} + \frac{\omega_p^2}{\omega^2}\right)^{1/2}. \tag{68}$$

With this constraint, our approximations are valid at all angles at which there is significant radiation (see Fig. 2), and the right-hand side of Eq. (67) can be expanded in powers of the small quantity $\theta\tan\vartheta\cos\phi$. The leading term is independent of $\cos\phi$ and gives the same angular distribution for the transition radiation about the line of flight of the particle as was obtained for normal incidence on the slab. The first correction term introduces a cos ϕ dependence, but its contribution to $d^2\mathcal{E}/d\omega d\phi$ is only of order $\bar{\theta}\tan\vartheta \ll 1$ relative to the leading term. (The radiation has a net linear polarization of the same order.) This correction drops out if the angular distribution is integrated over ϕ, and, as a consequence, the corrections to $d\mathcal{E}/d\omega$ and $d^2\mathcal{E}/d\omega d\theta$ associated with oblique incidence are at most of order $\bar{\theta}^2\tan^2\vartheta$.[24] These corrections are negligible under the conditions of interest. We conclude that the results of Sec. II can be used to describe the radiation emitted in the case of oblique incidence provided that the slab thickness a is replaced by $a/\cos\vartheta$, and the restrictions noted above are satisfied. Somewhat more detailed arguments show, in fact, that the azimuthally averaged distribution $d^2\mathcal{E}/d\omega d\theta$ is also unmodified in the high-energy, high-frequency limit by small departures from the plane parallel geometry assumed above, for example, surface roughness.[25]

B. Multiple foil arrangements

In this section we will consider the modifications of the results of Sec. II which arise when a single foil is replaced by a foil stack.[26] We will consider n parallel foils of thickness a separated by vacuum gaps of width b, and will restrict our arguments to the case of normal incidence of the particle beam. It is clear that the radiation field

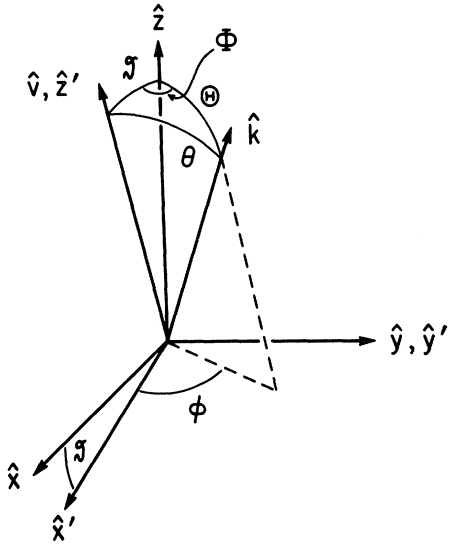

FIG. 9. The geometry used to describe the emission of transition radiation in the case of oblique incidence of a particle on a dielectric slab.

should approach that from a single foil of thickness na for $b \to 0$, and is plausible also that the intensity of the radiation should be n times that from a single radiator for b very large. Unfortunately, the situation of most interest for high-energy physics lies between these extreme limits and cannot be handled simply. The rather complicated variations of the radiation with frequency and angle of emission have been studied in detail for this case by Garibian.[26] We will therefore confine our attention primarily to the derivation of the basic equations and expressions for the frequency-averaged spectrum using our large-γ, high-frequency approximations.

The radiation from a foil stack is easily calculated by summing the fields radiated by the individual foils with the proper phase differences and the absorption in succeeding foils taken into account. We will initially neglect multiple reflections of the radiation in the foil stack and calculate only the direct radiation. We will take the origin of coordinates at the point at which the particle emerges from the foil stack, and will number the foils from 1 to n along the direction of the beam. The asymptotic vector potential is then given by the sum

$$\vec{A}_n(\vec{r}, \omega) \underset{r' \to \infty}{\sim} \sum_{m=1}^{n} e^{-i(n-m)(\phi_a + \phi_b) - (n-m)\lambda a/2}\, \vec{A}_1(\vec{r}', \omega) \tag{69a}$$

$$= \vec{A}_1(\vec{r}', \omega)[1 - e^{-in(\phi_a + \phi_b) - n\lambda a/2}] \times (1 - e^{-i\phi_a - i\phi_b - \lambda a/2})^{-1}, \tag{69b}$$

where

$$\phi_a = \left(\frac{\omega}{v} - \kappa_z\right) a \sim \frac{\omega a}{2c}\left(\theta^2 + \frac{1}{\gamma^2} + \frac{\omega_p^2}{\omega^2}\right), \tag{70a}$$

$$\phi_b = \left(\frac{\omega}{v} - k_z\right) b \sim \frac{\omega b}{2c}\left(\theta^2 + \frac{1}{\gamma^2}\right), \tag{70b}$$

$$\omega/\omega_p \gg 1, \quad \gamma \gg 1, \quad \theta \ll 1,$$

and $\vec{A}_1(\vec{r}', \omega)$ is the potential set up by an ultrarelativistic particle on passing through a single foil, Eq. (13),

$$\vec{A}_1(\vec{r}', \omega) \underset{r' \to \infty}{\sim} \frac{i}{(2\pi)^{1/2}} \frac{e}{v} \frac{\omega}{c} \frac{\epsilon - 1}{(\omega/v) - \kappa_z} \frac{\vec{\kappa}_\perp}{\kappa_\perp^2 + (\omega/\gamma v)^2} \times (1 - e^{-i\phi_a - \lambda a/2}) \frac{e^{ikr'}}{r'} . \tag{71}$$

The corresponding result for the energy radiated per unit solid angle per unit frequency by a stack of n foils is given by[27]

$$\frac{d^2\mathcal{E}_n}{d\omega d\Omega} = \frac{d^2\mathcal{E}_1}{d\omega d\Omega} \left| \sum_{m=1}^{n} e^{-i(n-m)(\phi_a + \phi_b) - (n-m)\lambda a/2} \right|^2 \tag{72a}$$

$$= (d^2\mathcal{E}_0/d\omega d\Omega)(1 + e^{-\lambda a} - 2e^{-\lambda a/2}\cos\phi_a) \times \frac{1 + e^{-n\lambda a} - 2e^{-n\lambda a/2}\cos n(\phi_a + \phi_b)}{1 + e^{-\lambda a} - 2e^{-\lambda a/2}\cos(\phi_a + \phi_b)} , \tag{72b}$$

where

$$\frac{d^2\mathcal{E}_0}{d\omega d\Omega} = \frac{e^2}{\pi^2 c}\left(\frac{\omega_p}{\omega}\right)^4 \times \frac{\theta^2}{[\theta^2 + (1/\gamma^2) + (\omega_p^2/\omega^2)]^2[\theta^2 + (1/\gamma^2)]^2} . \tag{73}$$

This result for $d^2\mathcal{E}_n/d\omega d\Omega$ simplifies considerably in several limits. If b is sufficiently small that $n\phi_b \ll 1$, the b-dependent terms in Eq. (72b) can be dropped. The remaining expression is identical to that for a single foil of thickness na, Eq. (62). This simplification is associated physically with the fact that the radiation field in vacuum and the field of the incident charged particle remain in phase over distances greater than the total vacuum gap in the stack ($n\phi_b \ll 1$), and the radiation fields from successive foils add as if those foils were adjacent. If both a and b are small enough that $\phi_a < 1$, $\lambda a < 1$, and $\phi_b < 1$ (thin foils and narrow gaps), the foil stack acts as a single foil with a thickness $n(a+b)$ and an average high-frequency dielectric susceptibility reduced by the ratio $a/(a+b)$ of the thickness of material to the total thickness,

$$\frac{\omega_p^2}{\omega^2} \to \frac{a}{a+b}\frac{\omega_p^2}{\omega^2} . \tag{74}$$

The resulting expression for $d^2\mathcal{E}_n/d\omega d\Omega$ can be obtained by making these replacements in Eq. (62). We will not consider these limits further, as they are not of interest for applications of transition radiation to high-energy physics. We will therefore assume in the remaining discussion that $\phi_a > 1$ and $\phi_b > 1$.

It is clear from Eqs. (62) and (72b) that the transition radiation from a foil stack is effectively confined to a cone $\theta \lesssim \bar{\theta}$ with the same opening angle $\bar{\theta}$ as the radiation from a single foil, Eq. (27). However, the distribution of the radiation inside this cone is modulated by the extra factor which appears in Eq. (72b). If the absorption in a single foil is small, this factor is sharply peaked at angles such that $\phi_a + \phi_b = 2m\pi$, $m = 1, 2, \ldots$, and is small elsewhere. As a result, the radiation is actually emitted in a set of coaxial cones with individual opening angles $\theta_1 < \theta_2 < \cdots < \bar{\theta}$. This redistribution of the radiation in angle has, as we shall see, rather little effect on the total energy emitted. The angular distribution has been considered in detail by Garibian.[26] We will consider only the spectrum integrated over all angles of emission, $d\mathcal{E}_n/d\omega$.

It will be useful for our purposes to rewrite Eqs. (72b) in an alternative form which can be obtained by straightforward manipulation of Eq. (72a),

$$\frac{d^2\mathcal{E}_n}{d\omega d\Omega} = \frac{d^2\mathcal{E}_1}{d\omega d\Omega} \frac{1 - e^{-n\lambda a}}{1 - e^{-\lambda a}}\left[1 + 2\sum_{k=1}^{n-1} e^{-k\lambda a/2} \frac{1 - e^{-(n-k)\lambda a}}{1 - e^{-n\lambda a}} \cos k(\phi_a + \phi_b)\right] . \tag{75}$$

Here $d^2\mathcal{E}_1/d\omega d\Omega$ is the spectrum for a single foil, Eq. (62). The peaking in the angular distribution noted above results in this form from the coherent addition of all terms in the cosine series when $(\phi_a + \phi_b) = 2m\pi$. The angular integrals involved in the calculation of $d\mathcal{E}_n/d\omega$, the frequency spectrum of the radiation, can all be evaluated in terms of sine- and cosine-integral functions. The results are similar to those in Sec. IIE, but are even less illuminating and will not be presented. However, they simplify considerably if $(\omega b/2\gamma^2 c) \gg 1$ at the frequencies of interest (the limit of very wide gaps). The cosine functions in Eq. (75) then undergo a number of oscillations in the angular interval in which $d^2\mathcal{E}_1/d\omega d\Omega$ is large, and tend to average to zero in the angular integration. As a result,

$$\frac{d\mathcal{E}_n}{d\omega} \to \frac{d\mathcal{E}_1}{d\omega}\frac{1 - e^{-n\lambda a}}{1 - e^{-\lambda a}} , \quad \omega b/2\gamma^2 c \gg 1 . \tag{76}$$

The expression for $d\mathcal{E}_1/d\omega$ is given in Eq. (63).

If the gaps in the foil stack are wide, but not very wide, $(\omega b/2c)\theta_{max}^2 \gg 1$ and $(\omega b/2\gamma^2 c) \gtrsim 1$, the cosine terms in Eq. (75) do not average to zero in the angular integration for small values of the summation index k, but lead to terms in $d\mathcal{E}_n/d\omega$ which oscillate rapidly with ω for frequencies $\omega \ll \gamma\omega_p$.[28] While there is then no simple expression for $d\mathcal{E}_n/d\omega$, an investigation similar to that at the end of Sec. II E indicates that Eq. (76) may still be used to calculate either $\mathcal{E}_n(\omega > \omega_0)$ or the frequency averaged spectrum $(d\mathcal{E}_n/d\omega)_{av}$ provided the range of integration or averaging includes many periods of oscillation. (This restriction will not be satisfied, for example, if a lower cutoff frequence ω_0 imposed by absorption of the radiation in the foils restricts the effective range of integration to the region $\omega \gtrsim \gamma\omega_p$.) In this limit, the effects of the cosine series in Eq. (75) are confined to the details of the angular and frequency distributions of the transition radiation. Both are modified, but the average properties of the radiation are essentially unchanged. The effects of the vacuum gaps can be minimized in practice by making b as large as possible, with the minimum gap size determined by the condition that $b > (2\gamma^2 c/\omega)$ for the lowest frequency to be detected, e.g., $b > 1.3 \times 10^{-8}\gamma^2$ cm for $\hbar\omega \gtrsim 3$ keV.

If both the thick-foil condition $a > (2\gamma c/\omega_p)$ and the wide-gap condition $b > (2\gamma^2 c/\omega)$ are satisfied, the average frequency spectrum may be approximated as

$$\left(\frac{d\mathcal{E}_n}{d\omega}\right)_{av} \approx \frac{2e^2}{\pi c}\bar{n}(\omega)F(x), \tag{77}$$

where $F(x)$ is defined in Eq. (35), and the effective number of foils in the stack at frequency ω is given by

$$\bar{n}(\omega) = \frac{1 - e^{-n\lambda a}}{1 - e^{-\lambda a}} . \tag{78}$$

If the entire stack is optically thick to the radiation $(n\lambda a \gg 1)$, but the individual foils are thin $(\lambda a \ll 1)$, $\bar{n} \sim (\lambda a)^{-1} = L/a$, where $L(\omega)$ is the mean absorption length for radiation of angular frequency ω. That is, the effective number of foils is just the number necessary to give one absorption length of material. If the entire stack is optically thin, $\bar{n}(\omega) \sim n$ as expected. Since the absorption increases strongly with decreasing ω ($\lambda/\rho \sim 2070E^{-3}$ g cm^2 for polypropylene in the 2–10 keV range, E in keV), the ratio $\bar{n}(\omega)/n$ drops rapidly at low frequencies [frequencies such that $na \gg L(\omega)$]. The low-frequency radiation from stacks with a large number of foils is therefore strongly suppressed. The details depend on the number of foils and the material used. The total energy radiated for different values of γ can be calculated approximately by integrating Eq. (77), with the frequency dependence of $\bar{n}(\omega)$ taken into account.

C. Internal reflections in foil stacks

We have so far ignored multiple reflections of the transition radiation inside the foil stack. Some radiation will be reflected at each surface, and the resulting changes in the intensity of the transmitted radiation can be important at optical frequencies. However, these effects are quite small at the frequencies of interest even for a rather large number of foils.

The simplest effect involves the losses caused by incoherent reflection of the radiation emitted in the mth foil back into the stack at the surfaces of the succeeding $(n - m)$ foils. This results in a reduction of the amplitude of the radiation field by a factor

$$(T_i T_0)^{n-m}, \tag{79}$$

where T_i and T_0 are the transmission amplitudes (ratios of transmitted to incident amplitudes) for electromagnetic waves polarized in the plane of incidence for passage into and out of the foils,

$$T_i = \frac{2\cos\theta}{\epsilon^{1/2}\cos\theta + \epsilon^{-1/2}(\epsilon - \sin^2\theta)^{1/2}} \sim \frac{2}{\epsilon^{1/2}+1}\left(1 + \frac{\epsilon - 1}{4\epsilon}\tan^2\theta + \cdots\right), \quad |\epsilon - 1|, \theta \ll 1, \tag{80a}$$

$$T_0 = \frac{2(\epsilon - \sin^2\theta)^{1/2}}{\epsilon^{1/2}\cos\theta + \epsilon^{-1/2}(\epsilon - \sin^2\theta)^{1/2}} \sim \frac{2\epsilon}{\epsilon^{1/2}+1}\left(1 - \frac{\epsilon - 1}{4\epsilon}\tan^2\theta + \cdots\right), \quad |\epsilon - 1|, \theta \ll 1. \tag{80b}$$

The product $T_i T_0$ is particularly simple for high frequencies and small angles, and is given through fourth order in the small quantities (ω_p/ω), θ by

$$T_i T_0 \sim 1 - \frac{1}{16}\left(\frac{\omega_p}{\omega}\right)^4 + \cdots \quad (\omega_p/\omega) \ll 1, \ \theta \ll 1. \tag{81}$$

The effect of the single incoherent reflections under these conditions is simply to replace the x-ray absorption coefficient λ in Eqs. (69) through (77) by an effective absorption coefficient λ',

$$\lambda' = \lambda + \frac{1}{8}\left(\frac{\omega_p}{\omega}\right)^4 \frac{1}{a} . \tag{82}$$

This correction and those associated with higher-order incoherent multiple reflections can be neglected if

$$\frac{n}{8}\left(\frac{\omega_p}{\omega}\right)^4 \ll 1. \tag{83}$$

A potentially more important effect arises from coherent multiple reflections in the stack. We will assume that ϕ_a and ϕ_b are sufficiently large that waves which differ in phase by multiples of these quantities may be considered as incoherent in the sense discussed in the preceding section, and will consider only double reflections. The reflection amplitudes R_i and R_0 for waves passing into and out of the foils are

$$R_i = -R_0 = \frac{\epsilon^{1/2}\cos\theta - \epsilon^{-1/2}(\epsilon - \sin^2\theta)^{1/2}}{\epsilon^{1/2}\cos\theta + \epsilon^{-1/2}(\epsilon - \sin^2\theta)^{1/2}} \sim -\frac{1}{4}\frac{\omega_p^2}{\omega^2}, \quad \theta \ll 1, \ \omega_p/\omega \ll 1 . \tag{84}$$

There are four possibilities for the amplitude $R_l R_{l'}$ of a doubly-reflected wave corresponding to the four choices of $l, l' = i, 0$ for reflection on passage into or out of a foil. The waves reflected twice from foils k intervals apart also acquired extra phases $\phi_{ii} = 2k\phi_b$, $\phi_{i0} = \phi_{0i} = 2k(\phi_a + \phi_b)$, and $\phi_{00} = 2k(2\phi_a + \phi_b)$ relative to the original waves. It is evident from the phases which appear in Eq. (69) that waves reflected twice in the (i, i) and $(0, 0)$ combinations cannot be coherent with any of the direct waves under the conditions noted above, and, consequently, cannot alter the intensity of the transition radiation to order R^2. However, the direct radiation from the mth foil will be coherent with radiation from the $(m+2k)$th foil which is reflected twice in either the $(i, 0)$ or the $(0, i)$ combination by foils k intervals apart in its passage out of the stack. When all possibilities are considered, the mth term in Eq. (69a) is modified for reasonably large n by a factor

$$1 + \tfrac{1}{2} R_i R_0 (n-m)^2 \approx 1 - \frac{1}{32}\left(\frac{\omega_p}{\omega}\right)^4 (n-m)^2 . \tag{85}$$

The energy radiated is decreased accordingly,

$$\left(\frac{d\mathcal{E}_n}{d\omega}\right)_{av} \approx \frac{d\mathcal{E}_1}{d\omega}\left[\bar{n} - \frac{1}{16}\left(\frac{\omega_p}{\omega}\right)^4 \overline{n^3} + \cdots\right], \tag{86}$$

where $\overline{n^3} = \frac{1}{3}n^3$ in the limit of little absorption, and $\overline{n^3} = 2(L/a)^3$ for strong absorption. It is easy to check that this loss in the energy radiated in the forward direction is accounted for by the coherent single reflection of energy backwards out of the stack.

The coherent double-scattering correction in Eq. (87) will be unimportant if $n \ll 4\omega^2/\omega_p^2$ ($n \ll 4400$ for $\hbar\omega > 1$ keV, $\hbar\omega_p = 30$ eV). The remaining coherent higher-order multiple-scattering corrections are negligible under the same condition.[29] We conclude, as would be expected, that multiple internal reflections of high-frequency transition radiation are unimportant and can be neglected.

---

*Work supported by funds granted by the U. S. Atomic Energy Commission under Contract No. AT(11-1)-881.

[1]V. L. Ginzburg and I. M. Frank, Zh. Eksp. Teor. Fiz. 16, 15 (1946).

[2]G. M. Garibian, Zh. Eksp. Teor. Fiz. 37, 527 (1959) [Sov. Phys.—JETP 10, 372 (1960)].

[3]C. L. Wang, G. F. Dell, Jr., H. Uto, and L. C. L. Yuan, Phys. Rev. Lett. 29, 814 (1972); L. C. L. Yuan, C. L. Wang, H. Uto, and S. Prünster, Phys. Lett. 31B, 603 (1970).

[4]A. I. Alikhanian, S. A. Kankanian, A. G. Oganessian, and A. G. Tamanian, Phys. Rev. Lett. 30, 109 (1973); A. I. Alikhanian, K. M. Arakina, G. M. Garibian, M. P. Lorikian, and K. K. Shikhliarov, *ibid.* 25, 635 (1970).

[5]S. A. E. Johansson, Astrophys. Lett. 9, 143 (1971); I. Lerche, Astrophys. J. 175, 373 (1972).

[6]R. Ramaty and R. D. Bleach, Astrophys. Lett. 11, 35 (1972); G. B. Yodh, X. Artru, and R. Ramaty, Astrophys. J. 181, 725 (1973); W. Watson, *ibid.* 182, 17 (1973); L. Durand, *ibid.* 182, 417 (1973).

[7]F. G. Bass and V. M. Yakovenko, Usp. Fiz. Nauk. 86, 189 (1965) [Sov. Phys.—Usp. 8, 420 (1965)].

[8]G. M. Garibian, in *Proceedings of the International Conference on Instrumentation for High Energy Physics, Frascati, Italy, 1973*, edited by S. Stipcich (Laboratori Nazionali del Comitato Nazionale per l'Energia Nucleare, Frascati, Italy, 1973).

[9]J. D. Jackson, *Classical Electrodynamics* (Wiley, New York, 1962), Eqs. 13.29 and 13.30.

[10]It is actually sufficient for our purpose to neglect the refraction at the surface and approximate $\vec{\kappa}$ as $(\epsilon)^{1/2}\vec{k}$.

[11]The emission of Čerenkov radiation in conjection with transition radiation is discussed in Ref. 7.

[12]V. E. Pafomov, Zh. Eksp. Teor. Fiz. 33, 1074 (1957) [Sov. Phys.—JETP 6, 829 (1958)].

[13]G. M. Garibian and G. A. Chalikian, Zh. Eksp. Teor. Fiz. 35, 1282 (1958) [Sov. Phys.—JETP 8, 894 (1959)].

[14]Bass and Yakovenko, Ref. 7, Eq. 1.17.

[15]It is stated in Ref. 2 that the fixed-angle frequency spectrum is rather flat from optical frequencies to a cutoff at $\sim \frac{1}{2}\omega_c$, and drops rapidly to zero thereafter. It is evident from Fig. 3, curve *a*, that this is a rather crude representation of the actual distribution. This remark has been taken by some later authors (e.g., Refs. 5 and 7) to apply not only to the fixed-angle frequency spectrum, but also to the spectrum obtained after integration over θ. The latter falls smoothly and extremely rapidly with increasing ω (Fig. 4).

[16]We have evaluated $d\mathcal{E}/d\theta$ by integrating Eq. (32) over the entire interval $0 \le \omega \le \infty$ rather than the restricted interval $\omega_p < \omega < \infty$ for which our derivation is valid. The error introduced by this approximation is negligible if $\omega_c \gg \omega_p$ and $\omega_0 \gg \omega_p$.

[17]K. Mitchell, Philos. Mag. 40, 351 (1949); *Handbook of Mathematical Functions*, edited by M. Abramowitz and

I. Stegun, National Bureau of Standards Applied Mathematics Series, No. 55 (U.S.G.P.O., Washington, D.C., 1964), Sec. 27.7. We follow the notation of the second reference. The function $L(z)$ considered by Mitchell is related to f by $L(z) = f(1-z)$. For $|z| < 1$,

$$L(z) = f(1-z) = \sum_{k=1}^{\infty} \frac{z^k}{k^2} .$$

The result in Eq. (44) can be put in a form convenient for numerical calculation by using the identity

$$f(z) = f\left(1 - \frac{1}{z}\right) - \frac{\pi^2}{6} + \tfrac{1}{2}\ln^2 z - \ln z \ln(z-1) .$$

For $z = 1 + x_0^{-2}$, $f(1-z^{-1})$ is given by the convergent power series

$$f\left(\frac{1}{1+x_0^2}\right) = \sum_{k=1}^{\infty} \frac{(-1)^k}{k^2} \left(\frac{x_0^2}{1+x_0^2}\right)^k .$$

[18] *Handbook of Mathematical Functions*, edited by M. Abramowitz and I. Stegun, National Bureau of Standards Applied Mathematics Series, No. 55 (U.S.G.P.O., Washington, D.C., 1964), Sec. 5.2.

[19] See, for example, Figs. 4–7 in Ref. 8.

[20] These absorption lengths were calculated using the measured mass absorption coefficients λ/ρ of 1740, 1040, 234, 69, and 8 cm^2/g for $E = 1.03$, 1.24, 2.07, 3.1, and 6.2 keV given by B. L. Henke, R. L. Elgin, R. E. Lent, and T. B. Ledingham, NORELCO Reporter XIV, 112 (1967), a calculated value $\lambda/\rho = 2$ cm^2/g for $E = 10$ keV, and a density $\rho = 0.9$ g/cm^3.

[21] The possibility of reducing this absorption by using thinner foils is limited by the strong suppression of the radiation by the formation zone effect for

$$a < \frac{c}{\omega}\left(\frac{1}{\gamma^2} + \frac{\omega_p^2}{\omega^2}\right) .$$

The optimum thickness of the foils depends both on the frequency of the radiation detected and on the number of foils in a stack.

[22] The case of oblique incidence is treated in the exact theory by G. M. Garibian, Zh. Eksp. Teor. Fiz. 38, 1814 (1960) [Sov. Phys.—JETP 11, 1306 (1960)].

[23] The limiting case $(1 - \theta \tan\vartheta \cos\phi) = 0$ corresponds in our small-θ approximation to $\cos\Theta = 0$,

$$\frac{\cos\theta}{\cos\vartheta} = \cos\theta - \sin\theta \tan\vartheta \cos\phi$$

$$\sim 1 - \theta \tan\vartheta \cos\phi , \quad \theta \ll 1$$

that is, to a wave vector $\hat{k}$ in the x–y plane.

[24] The integrals over ϕ can be evaluated exactly in the thick-slab limit using the identities

$$\int_0^{2\pi} \frac{d\phi}{a + b\cos\phi} = \frac{2\pi}{(a^2 - b^2)^{1/2}} ,$$

$$\int_0^{2\pi} \frac{d\phi}{(a + b\cos\phi)^2} = \frac{2\pi a}{(a^2 - b^2)^{3/2}} .$$

It is necessary for consistency in this calculation to retain some higher-order terms which were dropped in the transition from Eq. (60) to Eq. (62). The exact calculation does not change the conclusions above.

[25] See, for example, Refs. 6, 7, and 8.

[26] The problem is treated exactly by Ya. B. Feĭnberg and N. A. Khizhnyak, Zh. Eksp. Teor. Fiz. 32, 883 (1957) [Sov. Phys.—JETP 5, 720 (1957)], and by G. M. Garibian, *ibid.* 35, 1435 (1958) [*ibid.* 8, 1003 (1959)].

[27] This result may also be obtained by taking the appropriate limits in the exact expressions given in Ref. 26. See, for example, G.M. Garibian, Zh. Eksp. Teor. Fiz. 60, 39 (1970) [Sov. Phys.—JETP 33, 23 (1971)], Eqs. (1) and (5).

[28] See, for example, Figs. 12–16 in Ref. 8.

[29] This condition is equivalent to that used by Garibian, Ref. 27, to reduce his exact expression for $d^2\mathcal{E}_n/d\omega d\Omega$ to the form given here in Eq. (72).